IEEE Access
Multidisciplinary | Rapid Review | Open Access Journal

Received 7 December 2023, accepted 29 December 2023, date of publication 9 January 2024, date of current version 16 February 2024.

Digital Object Identifier 10.1109/ACCESS.2024.3351773

RESEARCH ARTICLE

Gastrointestinal Cancer Detection and Classification Using African Vulture Optimization Algorithm With Transfer Learning

AHMED S. ALMASOUD[1], MOHAMMED MARAY[2], HEND KHALID ALKAHTANI[3], FAIZ ABDULLAH ALOTAIBI[4], MRIM M. ALNFIAI[5], AND AHMED SAYED[6]

[1]Department of Information Systems, College of Computer and Information Sciences, Prince Sultan University, Riyadh 12435, Saudi Arabia
[2]Department of Information Systems, College of Computer Science, King Khalid University, Abha 62529, Saudi Arabia
[3]Department of Information Systems, College of Computer and Information Sciences, Princess Nourah bint Abdulrahman University, P.O. Box 84428, Riyadh 11671, Saudi Arabia
[4]Department of Information Science, College of Humanities and Social Sciences, King Saud University, Riyadh 11437, Saudi Arabia
[5]Department of Information Technology, College of Computers and Information Technology, Taif University, Taif 21944, Saudi Arabia
[6]Research Center, Future University in Egypt, New Cairo 11835, Egypt

Corresponding author: Mrim M. Alnfiai (m.alnofiee@tu.edu.sa)

The authors extend their appreciation to the Deanship of Scientific Research at King Khalid University for funding this work through large group Research Project under grant number (RGP1/153/44). Princess Nourah bint Abdulrahman University Researchers Supporting Project number (PNURSP2024R384), Princess Nourah bint Abdulrahman University, Riyadh, Saudi Arabia. Research Supporting Project number (RSPD2024R838), King Saud University, Riyadh, Saudi Arabia. This study is partially funded by the Future University in Egypt (FUE).

ABSTRACT Gastrointestinal (GI) cancer comprises esophageal, gastric, colon and rectal tumors. The diagnosis of GI cancer often relies on medical imaging modalities namely magnetic resonance imaging (MRI), histopathological slides, endoscopy, and computed tomography (CT) scans. This provides particular details about the size, location, and characteristics of tumors. The high death rate for GI cancer patients shows that it is possible to increase analysis for a more personalized therapy strategy which leads to improved prognosis and few side effects although many extrapolative and predictive biomarkers exist. Gastrointestinal cancer classification is a challenging but vital area of research and application within medical imaging and machine learning. Artificial intelligence (AI) based diagnostic support system, especially convolution neural network (CNN) based image examination tool, has enormous potential in medical computer vision. The study presents a GI Cancer Detection and Classification utilizing the African Vulture Optimization Algorithm with Transfer Learning (GICDC-AVOADL) methodology. The major aim of the GICDC-AVOADL model is to examine GI images for the identification of cancer. To achieve this, the GICDC-AVOADL method makes use of an improved EfficientNet-B5 method to learn features from input images. Furthermore, AVOA is exploited for optimum hyperparameter selection of the improved EfficientNet-B5 method. The GICDC-AVOADL technique applies dilated convolutional autoencoder (DCAE) For GI cancer detection and classification. A complete set of simulations was conducted to examine the enhanced GI cancer detection performance of the GICDC-AVOADL technique. The extensive results inferred superior performance of the GICDC-AVOADL algorithm over current models.

INDEX TERMS Computer-aided diagnosis, cancers, GI cancer, artificial intelligence, parameter tuning.

I. INTRODUCTION

Gastrointestinal (GI) cancer generally includes colorectal, gastric, oesophageal, pancreatic and liver cancers which are the foremost reason for cancer-related death globally [1]. It is highly predictable that with the development of GI cancer, more number of clinical imaging datasets grow. But manual reading can't able to handle this growth and the difference in knowledge between radiologists leads to a high rate of missed diagnoses as well as misdiagnoses [2]. Nowadays, there

The associate editor coordinating the review of this manuscript and approving it for publication was Gustavo Callico.

are numerous techniques accessible for initial diagnosis of GC, which include endoscopic diagnosis (chromoendoscopy (CE), magnifying endoscopy, endoscopic ultrasonography, general endoscopy, etc., tumour maker diagnosis (GC makers, gastrin 17, pepsinogen, etc.), histopathological diagnosis and imaging diagnosis (nuclear magnetic resonance, computed tomography examination, X-ray examination, etc). Moreover, these types of diagnostic methods have the following limitations: histopathological diagnosis needs aggressive examination & time time-consuming, the endoscopic diagnosis technique is personal, the analytical method needs specialized knowledge as well as training and then the imaging diagnosis cannot identify initial injuries [3]. Tumor makers are mainly utilized to value the therapeutic effect of GC but as a result, there is no useful tumor marker for GC. That is why an accurate method, rapid and objective must be developed for the initial diagnosis of GC [4].

The most common approaches implemented for image diagnosis are Machine learning (ML) and DL (DL) [5]. But both technologies contain different benefits and drawbacks. At present, there are numerous existing methods available which can be selected as well as applied easily. Existing models are very easy to use but this is not suitable for certain tasks, which leads to bad performance [6]. During the algorithm plan, the features and design of these models must be considered carefully to finish specific tasks for reducing unwanted computation time when maintaining high-output performance. The techniques with high-end performance are measured by the Area Under Receiver Operating Characteristic (AUROC) is not suitable for clinical purposes [7]. It is highly essential to know about the clinical requirements as well as the current suitability of AI which is a part of medical workflow.

The medical professionals are called the end users of this approach [8]. It is important to consider and improve a model according to their workflow and needs, while flexibility balance is also in need for clinical settings or other hospitals [9]. The real challenge is connected with developing AI-based tools for facilitating pathologists in their flow of work [10]. In Pathology, ML has various applications which range from the classification of disease to an intelligent system just by judging the patient's symptoms and then suggesting medicines [6]. DL is a subfield of ML that defines the learning techniques by the function and structure of the human brain [11]. To get improved design recognition abilities, DL employs the influence of Artificial Neural Network (ANN).

This study presents a GICDC-AVOADL algorithm. The chief goal of the GICDC-AVOADL model is to examine GI images for the identification of cancer. To achieve this, the GICDC-AVOADL method makes use of an improved EfficientNet-B5 model for learning features from the input images. Furthermore, AVOA can be used for optimum hyperparameter selection of improved EfficientNet-B5 model. The GICDC-AVOADL algorithm applies dilated convolutional autoencoder (DCAE) For GI cancer detection and classification. A complete set of simulations was conducted to examine the enhanced GI cancer recognition behavior of the GICDC-AVOADL technique.

II. RELATED WORKS

In [12], the Machine Learning (ML) technique is mainly used for quantitative and automated evaluation of TLS based on routine histopathology images. International prognostic/diagnostic study in the multicentre, an accessible ML model proposed as well as validated for enumeration, classification of TLSs and automated detection in hematoxylin-eosin–stained images. Sakr et al. [13] projected a lightweight and new DL technique based on the CNN technique. In this technique, histopathological image inputs are standardized into the CNN method, and then colon cancer (CC) recognition is implemented. The better performance of the proposed model was examined with widely obtainable histopathological image data and later compared with novel models for the classification of CC. In [14], Raman spectroscopy is used to determine GAC models and separate tumorous gastric mucosa from usual gastric mucosa. Then, a SENet-LSTM approach is designed to recognize the automatic detection of cancerous and normal GI which is pre-processed with Raman spectra. Raman spectral feature defined recognition and determines explaining aptitude of classification method.

Aslam et al. [15] proposed a novel technique for feature extraction by employing a stacked sparse autoencoder. A Softmax classification algorithm was combined with the developed technique of feature extraction to organize GI tumours from breath samples. AE with Softmax classification algorithm was cascaded for developing a deep stacked SAE (DSSAE)-NN after the end of imperfect training. At last, the NN was performed with the aid of labelled training information. Azar et al. [16] main aim is to determine the probable DL techniques for the classification of CC. There are many DL optimizers were discovered in this study namely Adamax, stochastic gradient descent (SGD), Nesterov, root mean square prop (RMSprop), AdaDelta, Adam optimizer (Nadam) and so on. The proposed model was compared with numerous methods for four CC datasets. In [17], authors have used a gene expression profiling dataset from the Cancer Genome Atlas (TCGA) method. The research picked up the gene module using the greatest cancer correlation by Weighted Gene Co-expression Network Analysis (WGCNA). For difference expression outcome, extracted from genes features by employing Least Absolute Shrinkage and Selection Operator (LASSO) system as well as with assistance of Lasso-extracted feature, combined genes into modules.

Maashi et al. [18] proposed an Anas Platyrhynchos Optimizer with the aid of the DL-based Gastric Cancer Classification (APODL-GCC) technique. Mainly, the APODL-GCC method employs a difference improvement model. Anas Platyrhynchos Optimizer (APO) and Neural Architectural search network plans are mainly employed for feature optimization and extraction. At last, the GC detection method is mainly performed by using the Deep Belief Network process.

Kim et al. [19] designed a procedure to classify noncancerous colon tissues and CC via a DL-based CNN method. Initially, the projected study image for the CNN technique, an image-based DL model used as a midinfrared spectrum. And then, it is developed with the CNN process. The ML-based SVM method produced biased outcomes when the Routine pathological slide, routine pathological slide and tissue microarray (TMA) were verified.

In [20], the author demonstrates that deep residual learning is forecast MSI directly in H&E histology that is ubiquitously obtainable. This methodology can offer immunotherapy to a greatly broader subset of patients with GI cancer. Wang et al. [21] present a DL technique to analyze lymph node WSIs for identifying lymph nodes and tumor regions, and after that to uncover the tumor-area-to-MLN-area ratio (T/MLN). Baradaran Rezaei et al. [22] purposes at generating an Ensemble Method simulated in ML for predicting the most important aspects of the GC occurrence. The major objective of this research is to forecast the probabilities of GC existence and its connected deaths. Jin et al. [23] derive this case to establish a DL approach to predict LNMs in several nodal stations depending on preoperative CT images in patients with GC.

In [24], the AVOA is a currently proposed metaheuristic procedure that replicates the consumption and movement forms of reliable African vultures. However, AVOA is incapable of cracking the separate search space, which stimulates us to improve the dual AVOA for feature selection issues in classification tasks. Xi et al. [25] developed BAVOA to resolve numerous optimizer issues, particularly separate optimization problems. In BAVOA, the X-shaped transfer function is initially approved to adapt the constant search space into the dual search space, and then an opposition-based learning plan and an enhanced multi-elite plan are also used to improve the optimization capacity of BAVOA. Ghafari and Mansouri [26] developed an Enhanced AVOA-based Task Scheduling Strategy (E-AVOA-TS) for fog-cloud computing. Through the presented strategy, every village learns from its neighbors rather than from all of its associates. In [27], a hybrid meta-heuristic (MH) algorithm has been proposed to plan the IoT needs in IoT-fog-cloud systems by utilizing an Aquila Optimizer (AO) and AVOA termed AO_AVOA.

An important research gap in the domain of GI Cancer Detection and Classification utilizing DL is the vital need for effectual hyperparameter tuning strategies. As DL approaches, particularly CNNs have demonstrated great promise in this field, the optimum configuration of hyperparameters for these methods remains an open challenge. The result of DL approaches heavily relies on hyperparameters namely learning rates, batch sizes, dropout rates, and network architecture choices. The recent methods frequently utilize manual or heuristic approaches for hyperparameter selection that could not be optimum for the difficult task of GI cancer detection. Consequently, there is a pressing need for innovative methods, like automated optimization algorithms or specialized approaches, to systematically and rigorously tune hyperparameters to higher the accuracy and reliability of DL-based GI cancer detection and classification approaches. Addressing this gap will significantly advance the field and enhance the clinical utility of such methods for early and accurate analysis. Then, this work utilizes an AVOA-based hyperparameter tuning process.

III. THE PROPOSED MODEL

In this article, we proposed a programmed GI cancer recognition based on the GICDC-AVOADL methodology. The main purpose of the GICDC-AVOADL method is to examine GI images for cancer detection. In the proposed GICDC-AVOADL algorithm, the three most important processes are involved namely improved EfficientNet-B5-based feature extractor, AVOA-based parameter tuning, and DCAE-based classification. Fig. 1 illustrates the entire process of the GICDC-AVOADL algorithm.

A. STRUCTURE OF IMPROVED EFFICIENTNET-B5

Initially, the GICDC-AVOADL technique makes use of an improved EfficientNet-B5 model to learn the features from the input images. EfficientNet-B5 can be enhanced through the AWP model to add perturbation to the weight model and input for increasing the performance of the model [28]. Deng et al. proposed Arcface a loss function used for face detection which adds cumulative angular margin between target weights and features and increases the classification boundary in angular space to increase inter-class variances and intra-class compactness.

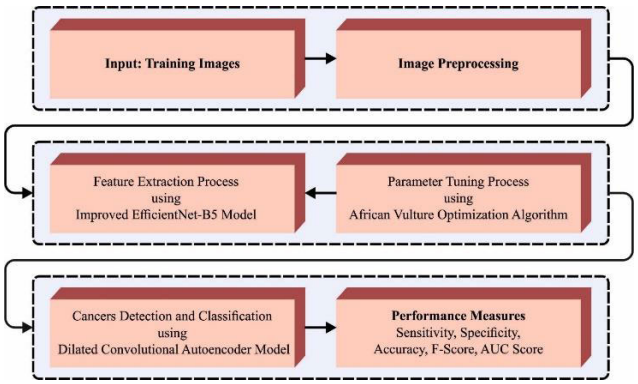

FIGURE 1. The overall process of the GICDC-AVOADL algorithm.

Due to its high similarity to different citrus leaf diseases, Arcface was used rather than softmax loss function. The specific formula for the softmax loss function is:

$$L_1 = -\frac{1}{N}\sum_{i=1}^{N}\log\frac{e^{W_{y_i}^T x_i + b_{y_i}}}{\sum_{j=1}^{n} e^{T_{x_i}+b_j}}, \quad (1)$$

In Eq. (1), a deep feature of samples related to the category y_i is x_i, a column of weight w is j, b_j refers to bias corresponding to w_j, the batch size is N, and the count of categories is n. The softmax loss function doesn't enhance

the embedding function to accomplish high similarity and diversity of samples within categories. First, set the bias b_j value to 0, and then the inner products of weight and input are formulated as follows:

$$W_j^T x_i = \|W_j\| \, \|x_i\| \, cos\theta_j \tag{2}$$

Processing w_j with L_2 regularization making $\|W_j = 1\|$, (L_2 regularization used to split value in w_j vector through the module of w_j to attain new w_j and module of new w_j is 1):

$$L_2 = -\frac{1}{N}\sum_{i-1}^{N} \log \frac{e^{\|x_i\| \cos(\theta_{y_i}))}}{e^{\|x_i\| \cos(\theta_{y_i}) + + \Sigma_{j=1, j\neq y_i}^{n} e^{\|x_i\| \cos\theta} j}} \tag{3}$$

Also, by multiplying by scale parameter s, the input x_i is regularized with L_2. The normalization stage of the feature and weight making the predictive relies only on the angle among the features as well as weights. Accordingly, embedding features learned are dispersed on the hypersphere of s radius. Since the embedding feature is disseminated near the centre of all features on the hypersphere, add cumulative angular margin among x_i and y_i to improve inter-class variance and intra-class compactness:

$$L_3 = -\frac{1}{N}\sum_{i=1}^{N} \log \frac{e^{s(\cos(\theta_{y_i} + m))}}{e^{s(\cos(\theta_{y_i} + m))} + \Sigma_{j=1, j\neq y_i}^{n} e^{s\cos\theta_j}} \tag{4}$$

Wu et al. proposed an adversarial training mechanism (AWP) to enhance the generalization capability of the model, which can enhance the robustness and regularize parameters. The weight loss landscape (WLL) represents the difference (generalization gap between the accuracy of the testing and training sets) under the training scenario. The dual perturbation model is formed due to AWP controlling the flatness of WLL in adversarial training, viz., adversarial perturbation input and weights:

$$\min_{w} \rho(w), \rho(w) = \frac{1}{n}\sum_{i=1}^{n} \max_{\|x_i' - x_i\|_p \leq \in} \ell(f_w(x_i'), y_i) \tag{5}$$

In Eq. (5), the adversarial sample within the ball (surrounded by L_p parameter) positioned on the natural sample x_i is x_i', number of training samples is n, standard classification loss is $\updownarrow$ (), adversarial loss is $\rho(w)$, and DNN with weight w is f_w.

B. PARAMETER TUNING PROCESS

In this phase, AVOA is employed for optimum hyperparameter selection of enhanced EfficientNet-B5 architecture. The hyperparameters, including the learning rate, number of epochs, and batch size, considerably affect the training dynamics and complete performance of the DL method. AVOA, enthused by the foraging behavior of African vultures, excels in enhancing these hyperparameters by logically traveling the search space, and professionally narrowing depressed optimum outlines. The learning rate, leading the step size at the time of gradient descent, and the number of epochs, central to the training iterations, are vital for attaining convergence and averting overfitting. Concurrently, the batch size, defining the number of data samples managed in every iteration, affects computational efficacy and memory usage. AVOA's capability to adjust and converge near an optimum set of hyperparameters improves the efficacy and value of the improved EfficientNet-B5 design, donating considerably to the better performance experimental in the GICDC-AVOADL model.

AVOA is a new intelligent optimizer technique whose main simulation comes from the foraging strategy and lifestyle of African vultures [29]. An algorithm shows fast convergence speed and strong optimization ability. The mathematical vector represents the individual vulture position within the population:

$$X = [X_1, X_2, \ldots, X_i, \ldots, X_n]^T \tag{6}$$

In Eq. (6), the location of i^{th} individual in the population is X_i, and the number of individuals in a population is n. The iterative process of AVOA is formulated as follows:

Phase 1: Population grouping and detection of an optimum vulture. The fitness of each individual considered after population initialization is generated. The individual location corresponding to suboptimal fitness values is considered a suboptimal location, whereas the individual location corresponding to the optimum fitness values is considered an optimum vulture location. Using Eqs. (7) and (8), the remaining vulture moves toward the optimum and suboptimal positions in the computation process for the selection possibility of the optimum vulture.

$$R(t) = \begin{cases} BestVulture_1 p_i = L_1 \\ BestVulture_2 p_i = L_2 \end{cases} \tag{7}$$

$$p_i = \frac{F_i}{\sum_{i=1}^{n} F_i} \tag{8}$$

where optimal and suboptimal vulture positions are $BestVulture_1$ and $BestVulture_2$. The selection probability of $BestVulture$ is p_i. The fitness value of other individuals is denoted by F_i. The existing iteration count is t. L_1 and L_2 are the parameters range within [1, 0]. The sum of L_1 and L_2 is often equivalent to 1. When L_2 approaches 0 and L_1 approaches 1, then the search capability of the model can be improved, which makes it more capable of finding local solutions. At the same time, when L_2 approaches 1 and L_1 approaches 0, it increases the search diversity, which makes it more capable of finding the global optimum solution.

Phase 2: Define the hunger rate of a vulture. A vulture in a hungry state conserves energy by remaining closer to a strong vulture and finding only nearby food. At the same time, the individual vultures have sufficient energy to fly long distances to find food. Additionally, a vulture in a hungry state exhibits the aggressive behaviors that are given below:

$$F = (2 \times rand_1 + 1) \times z \times \left(1 - \frac{t}{T}\right) + h\left[\sin^{\omega}\left(\frac{\pi}{2} \times \frac{t}{T}\right) + \cos\left(\frac{\pi}{2} \times \frac{t}{T}\right) - 1\right] \tag{9}$$

In Eq. (9), the maximal iteration counter is represented as T; the hunger rate of the vulture is F; $rand_1 \in (0, 1\ z \in (-1, 1)$ changes with all the iterations. Once the z value increases to 0, then the vulture is full. Once it drops below 0, then the vulture is in a hungry state. Before the optimization operation, a parameter ω is set. The value of ω enhances the possibility of entering the exploration phase at the last optimizer phase; or else, the probability reduces.

Phase 3: Exploration phase. The individual vulture can forage through two dissimilar strategies based on the user-defined parameter p_1 ($p_1 \in (0, 1)$), it chooses the strategy mode. This phase is denoted as follows:

$$P(i+1) = \begin{cases} R(i) - D(i)F & P_1 \geq rand_{p_1} \\ R(i) - F + rand_2 & \\ [(ub - lb)\, rand_3 + lb] & P_1 \leq rand_{p_1} \end{cases} \tag{10}$$

$$D(i) = |XR(i) - P(i)| \tag{11}$$

Here the vulture's position in the t^{th} and $t+1$ iterations are $P(i+1)$ and $P(i)$, correspondingly. X shows the coefficient vector that increases the random movement and changes in all the iterations. X is computed as 2 multiplied by the random integer within [1, 0]. The selection parameter of the exploration stage is represented as P_1. $rand_1$, $rand_2$, and $rand_{p_1}$ are random integer values ranging from zero to one. u_b and l_b refer to the upper and lower limits of the search range.

Phase 4: Exploitation phase. If $|F|$ is less than 1, then it enters the exploitation phase. The key value for selecting that approach is $|F| = 0.5$. If $|F| \geq 0.5$, the arithmetical expression stimulates features of spiral flight and performs as follows:

$$P(i+1) = \begin{cases} D(i)(F + rand) - d(t) & P_2 \geq rand_{p_2} \\ R(i) - (S_1 + S_2) & P_2 \leq rand_{p_2} \end{cases} \tag{12}$$

$$d(t) = R(i) - P(i) \tag{13}$$

$$S_1 = R(i)\frac{rand_5 P(i)}{2\pi}\cos P(i) \tag{14}$$

$$S_1 = R(i)\frac{rand_6 P(i)}{2\pi}\sin P(i) \tag{15}$$

where $rand_4$, $rand_5$, $rand_6$, *and* $rand_{p_2}$ are randomly created values lie in [1, 0], and the remaining parameters have a similar meaning.

If $|F|$ is lesser than 0.5, then the individual experiences hunger and fatigue that emulates its gathering behaviors and triggers aggressive behaviors. These behaviors are shown below:

$$P(i+1) = \begin{cases} \dfrac{(A_1 + A_2)}{2} & P_3 \geq rand_{p_3} \\ R(i) - |d(t)| & \\ FLevy(d) & P_3 \leq rand_{p_3} \end{cases} \tag{16}$$

$$A_1 = BestVulture_1(i) - \frac{BestVulture_1(i) \times P(i)}{BestVulture_1(i) \times P(i)^2} \times F \tag{17}$$

$$A_2 = BestVulture_2(i) - \frac{BestVulture_2(i) \times P(i)}{BestVulture_2(i) \times P(i)^2} \times F \tag{18}$$

where $rand_{p_3}$ signifies a random integer within [1, 0]. $BestVulture_1(i)$ and $BestVulture_2(i)$ are the optimum and sub-optimum locations of the vulture in the existing iteration. $Levy(d)$ signifies the stochastic model that emulates random walking, which influences the stepsize of vultures in the population. The fitness selection is a crucial factor in the AVOA approach. Solution encoding is exploited for assessing the aptitude (goodness) of the candidate solution. Now, the accuracy value is the main condition utilized for designing a fitness function.

$$Fitness = \max(P)$$
$$P = \frac{TP}{TP + FP} \tag{19}$$

From the expression, TP represents the true positive and FP denotes the false positive value.

C. DETECTION USING THE DCAE MODEL

The GICDC-AVOADL technique applied the DCAE model for GI cancer detection and classification. DCAE plays a vital part in GC recognition and classification by leveraging its innovative abilities in the extraction of feature and representation learning. The model's execution of DCAE improves its sensitivity to understated patterns suggestive of GI cancers, donating to the complete accuracy and reliability of the recognition procedure. This combination underlines the model's efficiency in finding tricky details within medical images, finally leading to enhanced diagnostic results in the realm of GC.

Like traditional AE, the dilated convolutional AE (DCAE) has a similar architecture [30]. Fig. 2 demonstrates the basic structure of DCAE. Through an activation function, the input is mapped into a feature map as given below.

$$h^k = f\left(x * W^k + b^k\right), \tag{20}$$

In Eq. (19), 2D input reshaped from a numeric vector is x, and the weighted matrix and bias equivalent to the k^{th} mapping feature h^k are W^k and b^k, correspondingly. $f(x) = (0,x)$ where $f(\cdot)$ is the ReLU activation function. The dilated convolution operator can be represented by the symbol $*$. Consequently, the feature map of HL is mapped to the reconstructed model via transposed convolution:

$$\tilde{x} = f\left(\sum_{k \in H} h^k * \tilde{W}^k + \tilde{b}\right), \tag{21}$$

In Eq. (19), the input x is similar to $\tilde{x}$ and H is a group of feature mappings. The primary values of W and $\tilde{W}$ weight matrices are the same. The learning objective of DCAE is to diminish the divergence between the reconstructed $\tilde{x}$ and the input x. Mean squared error (MSE) is the cost function:

$$L(x, \tilde{x}) = \frac{1}{n}\sum_{i}^{n}(x_i - \tilde{x}_i)^2 \tag{22}$$

Similar to SAEs, the DCAE constructs a DNN by stacking multiple DCAEs. Particularly, the hidden-layer output of the prior DCAE is the input of the next DCAE. Without losing information, dilated convolution may have a broader spectrum of receptive fields is one of the advantages of dilated convolution. These advantages make it better for text processing.

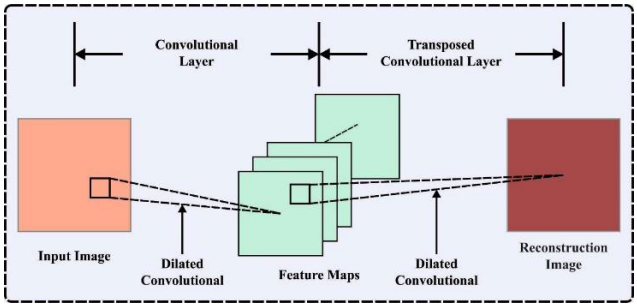

FIGURE 2. Structure of DCAE.

Briefly, the advantage of DCAE is as follows. Firstly, the applications of dilated convolution expand the receptive field of the layer to learn global features. In comparison to max−pooling, dilated convolution protects the input dataset from information loss. Next, the pre-training model of DCAEs does not need a labelled dataset that is more useful in practical applications. When compared to FCNNs, the DCAEs have fewer parameters. Thus, the DCAE is time-saving and more effective than other unsupervised DL algorithms.

IV. EXPERIMENTAL VALIDATION

In this section, GI cancer recognition outcomes of the GICDC-AVOADL technique are studied on the Kvasir dataset [31], comprising 5000 samples as well as five classes depicted in Table 1. The Kvasir database comprises images, annotated and verified by medical doctors (experienced endoscopists), containing many classes demonstrating anatomical landmarks, pathological findings or endoscopic procedures in the GI tract, i.e., hundreds of images for every class. The amount of images is adequate and utilized for various tasks, e.g., image retrieval, ML, DL, transfer learning (TL), and so on. The anatomical landmarks include Z-line, pylorus, cecum, etc., but the pathological finding comprises esophagitis, polyps, ulcerative colitis, etc. The dataset consists of images with distinct resolutions from 720×576 up to 1920×1072 pixels and is organized in a method but it can be sorted in separate folders named following this content.

Fig. 3 illustrates confusion matrices produced by the GICDC-AVOADL method under 80:20 and 70:30 of the TR phase/TS phase. The experimental values indicated effectual detection of all 5 classes.

In Table 2 and Fig. 4, GI cancer recognition outcomes of the GICDC-AVOADL model can be investigated under 80:20 of the TR Phase/TS Phase. The results pointed out GICDC-AVOADL technique categorizes all 5 samples proficiently. Meanwhile, On 80% of the TR Phase, the GICDC-AVOADL

TABLE 1. Details on database.

Labels	Classes	No. of Instances
C1	Dyed-Lifted Polyps	1000
C2	Normal-Cecum	1000
C3	Normal-Pylorus	1000
C4	Polyps	1000
C5	Ulcerative Colitis	1000
Total No. of Instances		5000

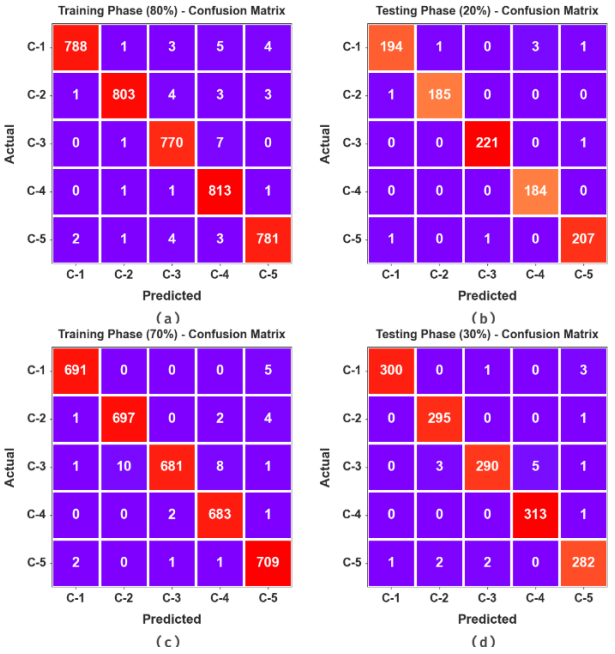

FIGURE 3. Confusion matrices of (a-c) TR phase of 80% and 70% and (b-d) TS phase of 20% and 30%.

technique reaches average $accu_y$, $sens_y$, $spec_y$, F_{score}, and AUC_{score} values of 99.55%, 98.88%, 98.87%, 98.87%, and 99.30% respectively. Also, on 20% of the TS Phase, the GICDC-AVOADL network offers an average $accu_y$, $prec_n$, $reca_l$, F_{score}, and AUC_{score} values of 99.64%, 99.09%, 99.11%, 99.09%, and 99.44% correspondingly.

In Table 3 and Fig. 5, GI cancer detection analysis of the GICDC-AVOADL technique was examined at 70:30 of the TR Phase/TS Phase. The resultant values denoted by GICDC-AVOADL technology categorize all 5 samples efficiently. Additionally, with70% of the TR Phase, the GICDC-AVOADL approach attains average $accu_y$, $sens_y$, $spec_y$, F_{score}, and AUC_{score} values of 99.55%, 98.89%, 99.72%, 98.89%, and 99.30% individually. Besides, with 30% of the TS Phase, the GICDC-AVOADL technique gives average $accu_y$, $prec_n$, $reca_l$, F_{score}, and AUC_{score} values of 99.47%, 98.66%, 99.67%, 98.66%, and 99.16% correspondingly.

To evaluate the performance of the GICDC-AVOADL technique under 80:20 of TR phase/TS phase, TR and TS $accu_y$ curves are defined, as illustrated in Fig. 6. The TR and TS $accu_y$ curves represent the behavior of

TABLE 2. GI cancer classifier outcome of GICDC-AVOADL algorithm at 80:20 of TR phase/TS phase.

Class	$Accu_y$	$Prec_n$	$Reca_l$	F_{score}	AUC_{score}
TR Phase (80%)					
Dyed-Lifted Polyps (C-1)	99.60	99.62	98.38	98.99	99.14
Normal-Cecum (C-2)	99.62	99.50	98.65	99.07	99.26
Normal-Pylorus (C-3)	99.50	98.47	98.97	98.72	99.30
Polyps (C-4)	99.48	97.83	99.63	98.72	99.53
Ulcerative Colitis (C-5)	99.55	98.99	98.74	98.86	99.24
Average	99.55	98.88	98.87	98.87	99.30
TS Phase (20%)					
Dyed-Lifted Polyps (C-1)	99.30	98.98	97.49	98.23	98.62
Normal-Cecum (C-2)	99.80	99.46	99.46	99.46	99.67
Normal-Pylorus (C-3)	99.80	99.55	99.55	99.55	99.71
Polyps (C-4)	99.70	98.40	100.00	99.19	99.82
Ulcerative Colitis (C-5)	99.60	99.04	99.04	99.04	99.40
Average	99.64	99.09	99.11	99.09	99.44

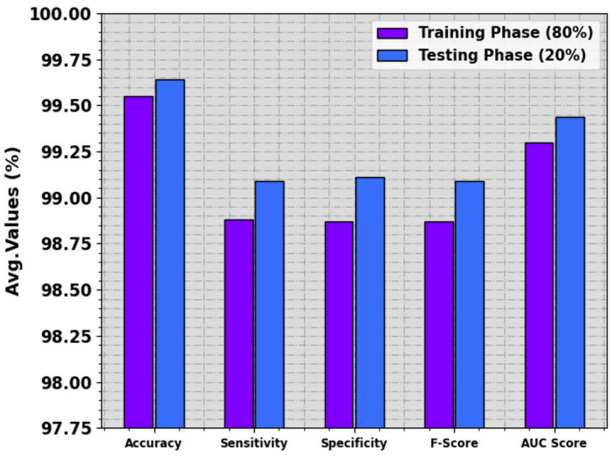

FIGURE 4. Average of GICDC-AVOADL algorithm at 80:20 of TR phase/TS phase.

the GICDC-AVOADL algorithm over diverse epochs. The figure proposes meaningful information regarding learning

TABLE 3. GI cancer classifier outcome of GICDC-AVOADL algorithm at 70:30 of TR phase/TS phase.

Class	$Accu_y$	$Prec_n$	$Reca_l$	F_{score}	AUC_{score}
TR Phase (70%)					
Dyed-Lifted Polyps (C-1)	99.74	99.28	99.86	99.35	99.57
Normal-Cecum (C-2)	99.51	99.01	99.64	98.80	99.32
Normal-Pylorus (C-3)	99.34	97.15	99.89	98.34	98.52
Polyps (C-4)	99.60	99.56	99.61	98.99	99.59
Ulcerative Colitis (C-5)	99.57	99.44	99.61	98.95	99.52
Average	99.55	98.89	99.72	98.89	99.30
TS Phase (30%)					
Dyed-Lifted Polyps (C-1)	99.67	98.68	99.92	99.17	99.30
Normal-Cecum (C-2)	99.60	99.66	99.58	98.99	99.62
Normal-Pylorus (C-3)	99.20	96.99	99.75	97.97	98.37
Polyps (C-4)	99.60	99.68	99.58	99.05	99.63
Ulcerative Colitis (C-5)	99.27	98.26	99.51	98.09	98.88
Average	99.47	98.66	99.67	98.66	99.16

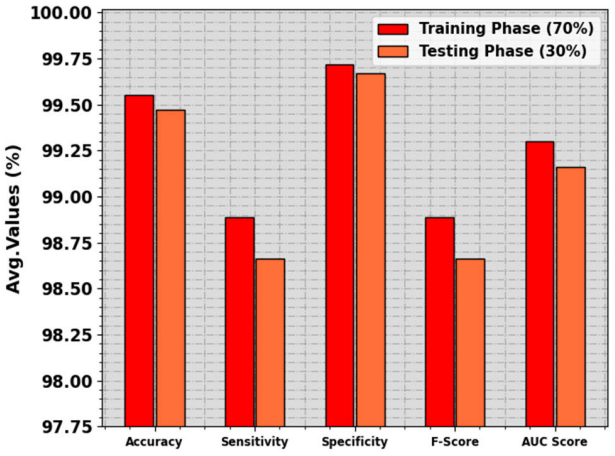

FIGURE 5. Average of GICDC-AVOADL algorithm at 70:30 of TR phase/TS phase.

tasks and simplification capabilities of the GICDC-AVOADL methodology. With a high rise in epoch count, it is observed that TR and TS $accu_y$ curves acquired improved. It is mentioned that the GICDC-AVOADL system accomplishes higher testing accuracy and can identify patterns in TR and TS data.

Fig. 7 exhibited inclusive TR and TS loss values of the GICDC-AVOADL approach under 80:20 of the TR phase/TS phase over epochs. The TR loss denotes method loss decreases over epochs. Mainly, loss values become decreased as the model modifies weight to decrease predicted error on TR and TS data. Loss curves specify the level where the model fits training data. It is noted that TR and TS loss

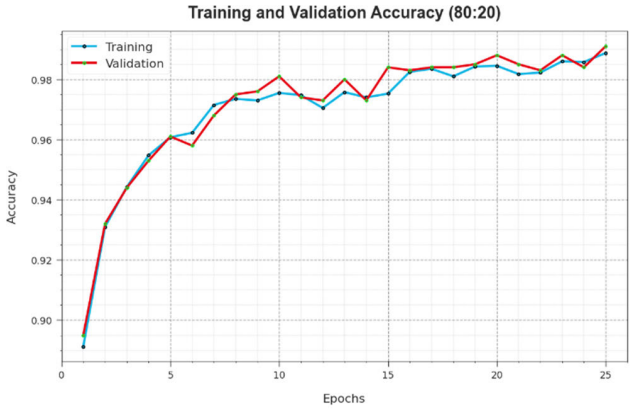

FIGURE 6. $Accu_y$ curve of GICDC-AVOADL algorithm on 80:20 of TR phase/TS phase.

FIGURE 7. Loss curve of GICDC-AVOADL system at 80:20 of TR phase/TS phase.

is gradually minimized and represented GICDC-AVOADL method positively learns patterns identified in TR and TS data. It is also demonstrated that the GICDC-AVOADL model differs in limitations for lessening alteration among predictive and definite training labels.

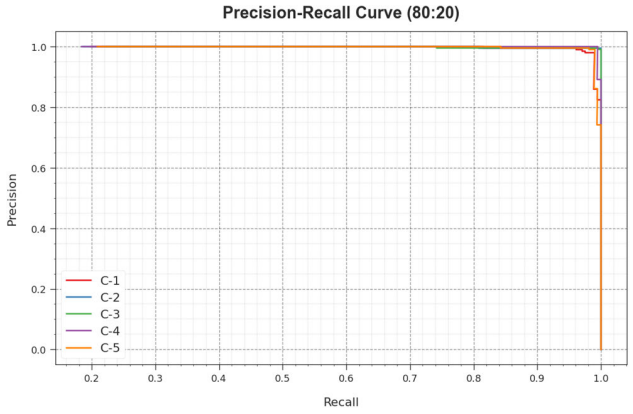

FIGURE 8. PR curve of GICDC-AVOADL methodology at 80:20 of TR phase/TS phase.

The PR analysis of the GICDC-AVOADL model at 80:20 of the TR phase/TS phase was established by scheming exactness against recall as denoted in Fig. 8. The experimental values confirm that the GICDC-AVOADL technique attains raised PR values on all 5 classes. The figure states that the model learns to identify different class labels. The GICDC-AVOADL technique reaches higher experimental values in the identification of optimistic samples with a decrease in wrong positives.

The ROC analysis produced by the GICDC-AVOADL method under 80:20 of the TR phase/TS phase is verified in Fig. 9, which has the aptitude of difference of class labels. The figure recognizes valued visions into trade-offs among TPR and FPR rates over various detection thresholds and changing numbers of epochs. It exhibits the exact analytical behavior of the GICDC-AVOADL model on the classification of 5 classes.

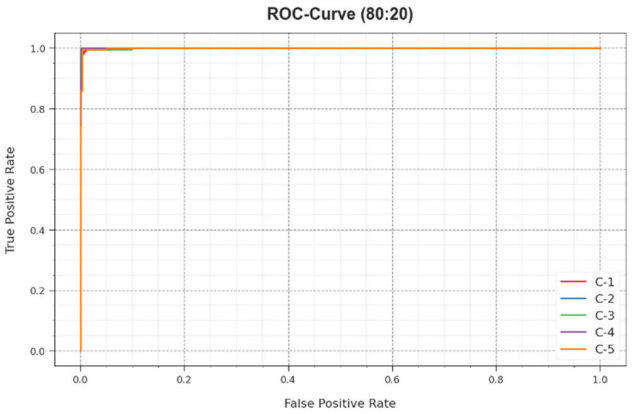

FIGURE 9. ROC curve of GICDC-AVOADL methodology on 80:20 of TR phase/TS phase.

To exhibit the promising performance of the GICDC-AVOADL method, an extensive range of experiments is performed in Table 4 [3], [32], [33], [34].

TABLE 4. Comparative outcome of GICDC-AVOADL approach with recent algorithms [3], [32], [33], [34].

Methods	$Accu_y$	$Sens_y$	$Spec_y$	AUC_{score}	CT (s)
GICDC-AVOADL	99.64	99.09	99.11	99.09	1.02
GDDC-HRODL	99.19	98.72	99.08	99.00	2.67
DL	97.35	96.74	97.03	98.69	3.89
Augmented CNN	99.00	98.68	97.70	96.05	3.16
AlexNet Model	96.43	97.64	99.01	98.59	4.23
GoogleNet Model	98.76	96.60	98.92	97.02	4.19
ResNet-50 Model	97.77	96.73	99.10	96.90	3.92

Fig. 10 represents a detailed comparison study of the GICDC-AVOADL technique. The simulation values indicate that the AlexNet approach reaches worse GI cancer classification outcomes. Next, the DL, GoogleNet, and ResNet-50 models obtain certainly improved performance. In the

meantime, the GDDC-HRODL and Augmented CNN models attain reasonable results. But the GICDC-AVOADL system demonstrates maximum results with an $accu_y$ of 99.64%, $sens_y$ of 99.09%, $spec_y$ of 99.11%, and AUC_{score} of 99.09%.

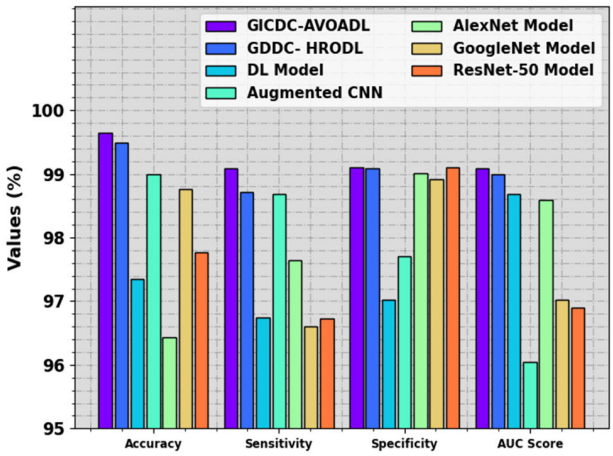

FIGURE 10. Comparative outcome of GICDC-AVOADL methodology with recent systems.

Finally, computation time (CT) results of the GICDC-AVOADL method with recent models are given in Fig. 11. The results highlighted that the GICDC-AVOADL approach provides minimal CT of 1.02s. At the same time, the GDDC-HRODL, DL, Augmented CNN, AlexNet, GoogleNet, and ResNet-50 models attain increased CT of 2.67s, 3.89s, 3.16s, 4.23s, 4.19s, and 3.92s correspondingly.

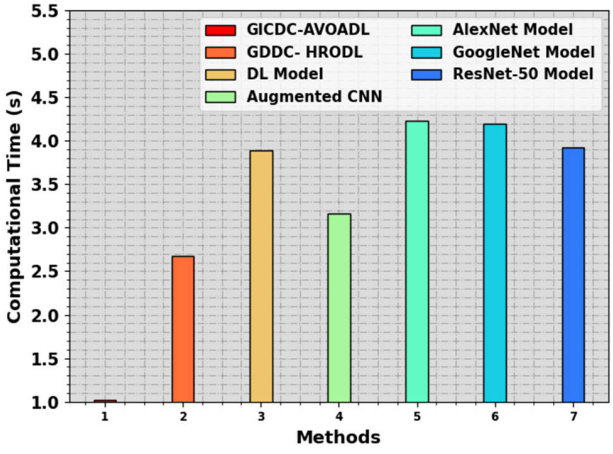

FIGURE 11. CT outcome of GICDC-AVOADL approach with recent algorithms.

These outcomes clearly stated that the GICDC-AVOADL methodology properly classified GI cancer.

V. CONCLUSION

In this research, we have proposed automated GI cancer detection utilizing GICDC-AVOADL technology. The purpose of the GICDC-AVOADL system is to study GI images for the detection of cancer. In the proposed GICDC-AVOADL algorithm, the three most important processes are involved namely improved EfficientNet-B5-based feature extractor, AVOA-based parameter tuning, and DCAE-based classification. A comprehensive set of simulations was conducted to examine the enhanced GI cancer detection performance of the GICDC-AVOADL method. The extensive results inferred superior performance of the GICDC-AVOADL algorithm over existing models with a maximum accuracy of 99.64%. By integrating DL with AVOA for hyperparameter tuning, the proposed model demonstrates superior performance in accurately identifying and classifying gastrointestinal cancers. This research holds better promise for enhancing diagnostic accuracy and ultimately improving patient performances from the context of GI cancer management.

Through its application of an improved EfficientNet-B5 design with enhanced hyperparameters courtesy of AVOA, the model not only attains greater accuracy in detecting and classifying GI cancers but also validates heightened efficacy in the procedure of diagnostic. The real-life effects of the GICDC-AVOADL technique are reflective, delivering clinicians a dominant tool for more exact and modified therapy plans, which leads to enhanced forecasts for patients. By improving the accuracy of medical imaging analysis, this technique has a high potential to transform medical decision-making in gastroenterology, simplifying initial recognition and involvement.

Future work for the GICDC-AVOADL approach involves extending its applicability to a wider range of GI diseases beyond cancer, comprising precancerous lesions and inflammatory conditions, to offer a further widespread diagnostic tool. Moreover, exploring the incorporation of multi-modal data, namely relating medical imaging with clinical data or genomics data can further improve the model's diagnostic abilities. At last, efforts to combine real-time endoscopic video analysis and execute the model from the clinical settings, to assist healthcare specialists in the processes, would be a crucial step near practical clinical adoption.

ACKNOWLEDGMENT

The authors extend their appreciation to the Deanship of Scientific Research at King Khalid University for funding this work through large group Research Project under grant number (RGP1/153/44). Princess Nourah bint Abdulrahman University Researchers Supporting Project number (PNURSP2024R384), Princess Nourah bint Abdulrahman University, Riyadh, Saudi Arabia. Research Supporting Project number (RSPD2024R838), King Saud University, Riyadh, Saudi Arabia. This study is partially funded by the Future University in Egypt (FUE).

REFERENCES

[1] Z. Guleken, P. Jakubczyk, W. Paja, K. Pancerz, A. Wosiak, I. Yaylım, G. I. Gültekin, N. Tarhan, M. T. Hakan, D. Sönmez, D. Sarıbal, S. Arıkan, and J. Depciuch, "An application of Raman spectroscopy in combination with machine learning to determine gastric cancer spectroscopy marker," *Comput. Methods Programs Biomed.*, vol. 234, Jun. 2023, Art. no. 107523.

[2] C. Li, Y. Qin, W. Zhang, H. Jiang, B. Song, M. R. Bashir, H. Xu, T. Duan, M. Fang, L. Zhong, L. Meng, D. Dong, Z. Hu, J. Tian, and J. Hu, "Deep learning-based AI model for signet-ring cell carcinoma diagnosis and chemotherapy response prediction in gastric cancer," *Med. Phys.*, vol. 49, no. 3, pp. 1535–1546, Mar. 2022.

[3] H. Hu, L. Gong, D. Dong, L. Zhu, M. Wang, J. He, L. Shu, Y. Cai, S. Cai, W. Su, Y. Zhong, C. Li, Y. Zhu, M. Fang, L. Zhong, X. Yang, P. Zhou, and J. Tian, "Identifying early gastric cancer under magnifying narrow-band images with deep learning: A multicenter study," *Gastrointestinal Endoscopy*, vol. 93, no. 6, pp. 1333–1341, Jun. 2021.

[4] X. Guan, N. Lu, and J. Zhang, "Computed tomography-based deep learning nomogram can accurately predict lymph node metastasis in gastric cancer," *Digestive Diseases Sci.*, vol. 68, no. 4, pp. 1473–1481, Apr. 2023.

[5] Y. Zhao, B. Hu, Y. Wang, X. Yin, Y. Jiang, and X. Zhu, "Identification of gastric cancer with convolutional neural networks: A systematic review," *Multimedia Tools Appl.*, vol. 81, no. 8, pp. 11717–11736, 2022.

[6] S. Kuntz, E. Krieghoff-Henning, J. N. Kather, T. Jutzi, J. Höhn, L. Kiehl, A. Hekler, E. Alwers, C. von Kalle, S. Fröhling, J. S. Utikal, H. Brenner, M. Hoffmeister, and T. J. Brinker, "Gastrointestinal cancer classification and prognostication from histology using deep learning: Systematic review," *Eur. J. Cancer*, vol. 155, pp. 200–215, Sep. 2021.

[7] H. Suzuki, T. Yoshitaka, T. Yoshio, and T. Tada, "Artificial intelligence for cancer detection of the upper gastrointestinal tract," *Digestive Endoscopy*, vol. 33, no. 2, pp. 254–262, Jan. 2021.

[8] P. Podder, S. Bharati, and M. R. H. Mondal, "10 automated gastric cancer detection and classification using machine learning," in *Artificial Intelligence for Data-Driven Medical Diagnosis*. Berlin, Germany: De Gruyter, 2021, pp. 207–224.

[9] M. Vania, B. A. Tama, H. Maulahela, and S. Lim, "Recent advances in applying machine learning and deep learning to detect upper gastrointestinal tract lesions," *IEEE Access*, vol. 11, pp. 66544–66567, 2023.

[10] P.-C. Chen, Y.-R. Lu, Y.-N. Kang, and C.-C. Chang, "The accuracy of artificial intelligence in the endoscopic diagnosis of early gastric cancer: Pooled analysis study," *J. Med. Internet Res.*, vol. 24, no. 5, May 2022, Art. no. e27694.

[11] E. Bostanci, E. Kocak, M. Unal, M. S. Guzel, K. Acici, and T. Asuroglu, "Machine learning analysis of RNA-seq data for diagnostic and prognostic prediction of colon cancer," *Sensors*, vol. 23, no. 6, p. 3080, Mar. 2023.

[12] Z. Li, Y. Jiang, B. Li, Z. Han, J. Shen, Y. Xia, and R. Li, "Development and validation of a machine learning model for detection and classification of tertiary lymphoid structures in gastrointestinal cancers," *JAMA Netw. Open*, vol. 6, no. 1, Jan. 2023, Art. no. e2252553.

[13] A. S. Sakr, N. F. Soliman, M. S. Al-Gaashani, P. Pławiak, A. A. Ateya, and M. Hammad, "An efficient deep learning approach for colon cancer detection," *Appl. Sci.*, vol. 12, no. 17, p. 8450, Aug. 2022.

[14] C. Li, S. Liu, Q. Zhang, D. Wan, R. Shen, Z. Wang, Y. Li, and B. Hu, "Combining Raman spectroscopy and machine learning to assist early diagnosis of gastric cancer," *Spectrochimica Acta A, Mol. Biomolecular Spectrosc.*, vol. 287, Aug. 2023, Art. no. 122049.

[15] M. A. Aslam, C. Xue, Y. Chen, A. Zhang, M. Liu, K. Wang, and D. Cui, "Breath analysis based early gastric cancer classification from deep stacked sparse autoencoder neural network," *Sci. Rep.*, vol. 11, no. 1, p. 4014, Feb. 2021.

[16] A. T. Azar, M. Tounsi, S. M. Fati, Y. Javed, S. U. Amin, Z. I. Khan, S. Alsenan, and J. Ganesan, "Automated system for colon cancer detection and segmentation based on deep learning techniques," *Int. J. Sociotechnol. Knowl. Develop.*, vol. 15, no. 1, pp. 1–28, Jul. 2023.

[17] Y. Su, X. Tian, R. Gao, W. Guo, C. Chen, C. Chen, D. Jia, H. Li, and X. Lv, "Colon cancer diagnosis and staging classification based on machine learning and bioinformatics analysis," *Comput. Biol. Med.*, vol. 145, Jun. 2022, Art. no. 105409.

[18] M. S. Maashi, Y. A. R. Ali, A. Motwakel, A. S. A. Aziz, M. A. Hamza, and A. A. Abdelmageed, "Anas platyrhynchos optimizer with deep transfer learning-based gastric cancer classification on endoscopic images," *Electron. Res. Arch.*, vol. 31, no. 6, pp. 3200–3217, 2023.

[19] I. G. Kim, "Classification of midinfrared spectra of colon cancer tissue using a convolutional neural network," Current Optics and Photonics, vol. 6, no. 1, pp. 92–103, 2022.

[20] J. N. Kather, A. T. Pearson, N. Halama, D. Jäger, J. Krause, S. H. Loosen, A. Marx, P. Boor, F. Tacke, U. P. Neumann, H. I. Grabsch, T. Yoshikawa, H. Brenner, J. Chang-Claude, M. Hoffmeister, C. Trautwein, and T. Luedde, "Deep learning can predict microsatellite instability directly from histology in gastrointestinal cancer," *Nature Med.*, vol. 25, no. 7, pp. 1054–1056, Jul. 2019.

[21] X. Wang, Y. Chen, Y. Gao, H. Zhang, Z. Guan, Z. Dong, Y. Zheng, J. Jiang, H. Yang, L. Wang, X. Huang, L. Ai, W. Yu, H. Li, C. Dong, Z. Zhou, X. Liu, and G. Yu, "Predicting gastric cancer outcome from resected lymph node histopathology images using deep learning," *Nature Commun.*, vol. 12, no. 1, p. 1637, Mar. 2021.

[22] H. Baradaran Rezaei, A. Amjadian, M. V. Sebt, R. Askari, and A. Gharaei, "An ensemble method of the machine learning to prognosticate the gastric cancer," *Ann. Operations Res.*, vol. 328, no. 1, pp. 151–192, Sep. 2023.

[23] C. Jin, Y. Jiang, H. Yu, W. Wang, B. Li, C. Chen, Q. Yuan, Y. Hu, Y. Xu, Z. Zhou, G. Li, and R. Li, "Deep learning analysis of the primary tumour and the prediction of lymph node metastases in gastric cancer," *Brit. J. Surg.*, vol. 108, no. 5, pp. 542–549, May 2021.

[24] K. Balakrishnan, R. Dhanalakshmi, and G. Seetharaman, "S-shaped and V-shaped binary African vulture optimization algorithm for feature selection," *Expert Syst.*, vol. 39, no. 10, Dec. 2022, Art. no. e13079.

[25] M. Xi, Q. Song, M. Xu, and Z. Zhou, "Binary African vultures optimization algorithm for various optimization problems," *Int. J. Mach. Learn. Cybern.*, vol. 14, no. 4, pp. 1333–1364, Apr. 2023.

[26] R. Ghafari and N. Mansouri, "E-AVOA-TS: Enhanced African vultures optimization algorithm-based task scheduling strategy for fog–cloud computing," *Sustain. Comput., Informat. Syst.*, vol. 40, Dec. 2023, Art. no. 100918.

[27] Q. Liu, H. Kosarirad, S. Meisami, K. A. Alnowibet, and A. N. Hoshyar, "An optimal scheduling method in IoT-Fog-Cloud network using combination of Aquila optimizer and African vultures optimization," *Processes*, vol. 11, no. 4, p. 1162, Apr. 2023.

[28] Q. Dai, Y. Guo, Z. Li, S. Song, S. Lyu, D. Sun, Y. Wang, and Z. Chen, "Citrus disease image generation and classification based on improved FastGAN and EfficientNet-B5," *Agronomy*, vol. 13, no. 4, p. 988, Mar. 2023.

[29] X. Chen, W. Cui, and T. Zhang, "AVOA-LightGBM power fiber optic cable event pattern recognition method based on wavelet packet decomposition," *Electronics*, vol. 12, no. 18, p. 3743, Sep. 2023.

[30] Y. Yu, J. Long, and Z. Cai, "Network intrusion detection through stacking dilated convolutional autoencoders," *Secur. Commun. Netw.*, vol. 2017, pp. 1–10, Nov. 2017.

[31] *Kvasir: A Multi-Class Image-Dataset for Computer Aided Gastrointestinal Disease Detection*. Accessed: Jul. 8, 2023. [Online]. Available: https://datasets.simula.no/kvasir/#download

[32] O. M. Mirza, A. Alsobhi, T. Hasanin, M. K. Ishak, F. K. Karim, and S. M. Mostafa, "Computer aided diagnosis for gastrointestinal cancer classification using hybrid Rice optimization with deep learning," *IEEE Access*, vol. 11, pp. 76321–76329, 2023.

[33] A. M. Godkhindi and R. M. Gowda, "Automated detection of polyps in CT colonography images using deep learning algorithms in colon cancer diagnosis," in *Proc. Int. Conf. Energy, Commun., Data Anal. Soft Comput. (ICECDS)*, Chennai, India, Aug. 2017, pp. 1722–1728.

[34] R. Fonollá, F. van der Sommen, R. M. Schreuder, E. J. Schoon, and P. H. de With, "Multi-modal classification of polyp malignancy using CNN features with balanced class augmentation," in *Proc. IEEE 16th Int. Symp. Biomed. Imag. (ISBI)*, Venice, Italy, Apr. 2019, pp. 74–78.